The time-dependent response of a two-basin ocean to a sudden surface temperature change

Chiung-Yin Chang, [a] Malte F. Jansen, [a]

[a] *Department of the Geophysical Sciences, University of Chicago, Chicago, Illinois*

Corresponding author: Chiung-Yin Chang, cychang@princeton.edu

Current affiliation: Program in Atmospheric and Oceanic Sciences, Princeton University, Princeton, New Jersey

ABSTRACT: Building on previous work using single-basin models, we here explore the time-dependent response of the Atlantic Meridional Overturning Circulation (AMOC) to a sudden global temperature change in a two-basin ocean-ice model. We find that the previously identified mechanisms remain qualitatively useful to explain the transient and the long term time-mean responses of the AMOC in our simulations. Specifically, we find an initial weakening of the AMOC in response to warming (and vice versa for cooling), controlled by the mid-depth meridional temperature contrast across the Atlantic basin. The long-term mean response instead is controlled primarily by changes in the abyssal stratification within the basin. In contrast to previous studies we find that for small-amplitude surface temperature changes, the equilibrium AMOC is almost unchanged, as the abyssal stratification remains similar due to a substantial compensation between the effects of salinity and temperature changes. The temperature-driven stratification change results from the differential warming/cooling between North Atlantic Deep Water and Antarctic Bottom Water, while the salinity change is driven by changes in Antarctic sea ice formation. Another distinct feature of our simulations is the emergence of AMOC variability in the much colder and much warmer climates. We discuss how this variability is related to variations in deep-ocean heat content, surface salinity, and sea ice in the deep convective regions, both in the North Atlantic and Southern Ocean, and its potential relevance to past and future climates.

1. Introduction

The global overturning circulation is a key feature of Earth's ocean, and studying its reorganization under various types of external forcing is a crucial step towards understanding past and future climates. In recent decades, substantial work has been put together to investigate this important topic using a hierarchy of numerical models of diverse complexity (e.g. Cessi 2019, and references therein). The present study builds upon some of this previous work, focusing on the response of the overturning circulation in an idealized two-basin coupled ocean-ice model to atmospheric temperature change.

Climatic change affects a number of ocean boundary conditions, including temperature, freshwater fluxes and wind stress. The change in global temperature is arguably the most fundamental and robust hallmark of climate change, yet the direct response to such forcing has received perhaps less attention in the ocean dynamics community than e.g. wind-stress changes over the Southern Ocean. A recent study by Jansen (2017, hereafter J17) examined the steady state climates in an idealized, single-basin, coupled ice-ocean model. The results showed that atmospheric cooling alone is enough to explain a shoaling of the Atlantic meridional overturning circulation (AMOC) during the Last Glacial Maximum, as suggested by proxy data (e.g. Curry and Oppo 2005; Lynch-Stieglitz et al. 2007; Burke et al. 2015). J17 argued the mechanism responsible for the change of the AMOC depth is the change in surface buoyancy flux at high latitudes in the Southern Ocean, which controls the abyssal stratification and sets the lower boundary condition for the AMOC (Jansen and Nadeau 2016). When the atmosphere cools, the surface buoyancy flux around Antarctica becomes more negative due to increased brine rejection from enhanced sea ice formation, which increases the abyssal stratification and leads to a shallower AMOC.

Extending the work of J17 on the steady state response to atmospheric temperature change, Jansen et al. (2018, hereafter JNM18) used a similar model setup to study the time-dependent response during the ocean's adjustment to a new steady state. They showed that the AMOC initially weakens and shoals under a sudden atmospheric warming, which is qualitatively consistent with CMIP simulations for the 21st century (e.g. Cheng et al. 2013), but opposite to the equilibrium response to warming in the same model. They argued that this initial, transient response is controlled by the relatively slow warming of the deep ocean temperature in the interior ocean compared to the North Atlantic deep convective region, which warms first, thus weakening the meridional

density gradient. The physical understanding that emerged from J17 and JNM18 is therefore that the transient circulation response to a global surface temperature change can be attributed to the change in the northern surface temperature, whereas the steady state response can be attributed to the change in the Southern Ocean buoyancy loss, primary controlled by the salinity flux associated with sea ice formation (c.f. Liu 2006).

The mechanisms proposed by J17 and JNM18 are based on simulations with a geometry that includes only an idealized Southern Ocean and a single basin, which may be thought of as an idealized representation of the Atlantic and Southern Ocean sector, thus lacking any linkages to the rest of the global ocean. A major focus of recent studies has been on studying the effect of inter-basin interactions, using simulations that include a second basin to explicitly simulate the (Indo-)Pacific ocean (e.g. Jones and Cessi 2016; Thompson et al. 2016; Ferrari et al. 2017). Using this two-basin geometry, Nadeau et al. (2019) and Baker et al. (2020) confirmed that Southern Ocean buoyancy loss remains an important factor in setting the depth of the AMOC in the equilibrium, via controlling the buoyancy contrast between North Atlantic Deep Water (NADW) and Antarctic Bottom Water (AABW) (Nadeau and Jansen 2020; Sun et al. 2020a). However, neither study addresses the time-dependent adjustment, nor do they explicitly consider the effect of global cooling on both temperature and sea ice changes [1]. Sun et al. (2020b) consider the time-dependent response to north Atlantic surface warming in a two basin model, and find a weakening and shoaling of the AMOC. However, because the warming is limited to the North Atlantic, the circulation remains weakened indefinitely, and the primary focus of the study is on the associated circulation changes in the Pacific and Southern Ocean.

In this study, we present a set of idealized two-basin simulations using a coupled ice-ocean model that is otherwise similar to the simulations of J17 and JNM18. We vary the atmospheric temperature to examine the transient and steady state AMOC responses in these simulations and describe the extent to which they can be explained by the mechanisms proposed by J17 and JNM18. We also investigate the internal AMOC variability seen in some of these simulations and discuss in how far the oscillations may be explained by mechanisms proposed in earlier studies that have identified similar oscillations in model simulations.

[1] Baker et al. (2020) explicitly considered the effect of sea ice changes in isolation by considering the ocean's response to a change in the freezing point, but not a change of global surface temperature, while Nadeau et al. (2019) use an ocean-only model, where surface buocancy is prescribed via a restoring condition.

2. Model setup and reference simulation

The simulations analyzed in this study are conducted using the Massachusetts Institute of Technology General Circulation Model (MITgcm; Marshall et al. 1997) with a setup that largely resembles the coupled ice-ocean model simulations analyzed in J17 and JNM18. The ocean model solves the primitive equations using a Boussinesq approximation and the sea ice model considers sea ice dynamics using a viscous-plastic rheology. As in J17, we use the Gent and McWilliams (1990) scheme to parameterize mesoscale eddy fluxes, and the diapycnal diffusivity (κ) is prescribed using a vertically varying profile based on the estimate of Nikurashin and Ferrari (2013) (Fig. 1a). All simulations use a tracer acceleration scheme (Bryan 1984) to allow for long model integration times. Additional shorter simulations for different time intervals were performed without tracer acceleration to ensure a negligible impact on the presented results.

The primary difference between our model setup and the one in J17 is the idealized basin geometry and boundary conditions. As discussed in section 1, J17 considers a single small basin to represent the Atlantic, whereas we use a two-basin configuration with a second, larger basin to represent the Pacific. Our two-basin ocean is 210° wide and has a depth of $4km$ everywhere except for a 2°-wide sill that blocks the re-entrant channel below $3km$ depth at $0°W$. The horizontal resolution is 2° and we use 29 vertical levels with uneven spacing from 20m at the surface to 200m in the abyss. For the surface momentum forcing, we prescribe a zonally symmetric zonal wind (u_a) and a meridional wind (v_a) that is non-zero only over the last two latitude grid points adjacent to the southern boundary of the channel. As in J17, the meridional wind has a wavenumber-$1/2$ zonal structure (maximizing at the center of the domain) and crudely represents the effect of katabatic winds blowing from Antarctica (Fig. 1b). We prescribe evaporation minus precipitation ($E-P$) to be independent of longitude in each basin but different between the two basins. The meridional structures of $E-P$ in the two basins are shown in Fig. 1c and have been chosen to mimic the simulated climatological sector-averaged $E-P$ in the ERA5 reanalysis although the magnitude of precipitation in the Southern Ocean is somewhat enhanced, which we found to be necessary to avoid unrealistically salty AABW in the reference climate. For the surface thermal forcing, we use a simple linear restoring boundary condition that relaxes the surface ocean/ice temperature to a prescribed effective atmospheric temperature (T_a). We keep T_a zonally symmetric and tune its meridional structure (Fig. 1d) to obtain a present-day-like surface climate (Fig. 2a).

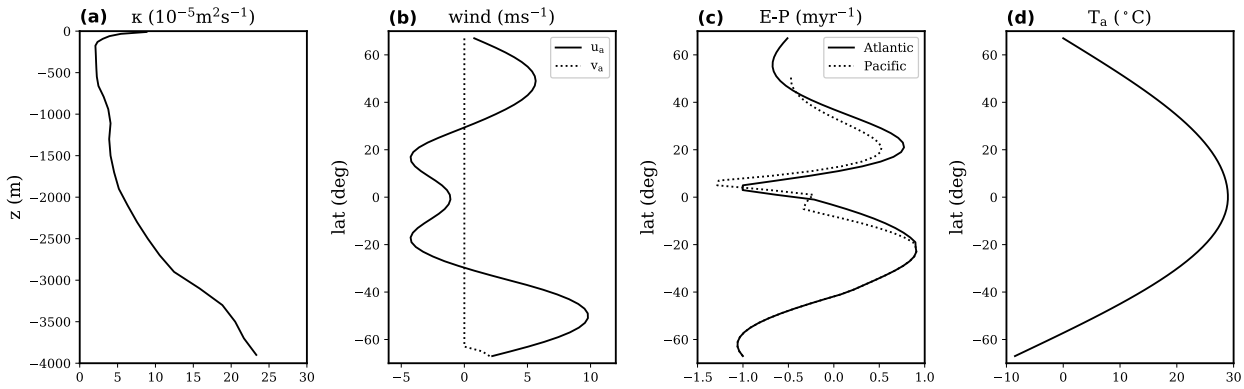

FIG. 1. The prescribed diapycnal diffusivity and surface forcing for the reference climate: (a) diapycnal diffusivty (κ; $10^{-5}m^2s^{-1}$) (b) zonal wind (u_a; ms^{-1}) and meridional wind (v_a; ms^{-1}) (c) evaporation minus precipitation ($E-P$; myr^{-1}), and (d) effective atmospheric temperature (T_a; $^\circ C$). The prescribed u_a and T_a are zonally symmetric, and $E-P$ is zonally symmetric within each basin. The prescribed v_a has a zonal wavenumber $1/2$ structure with the maximum (shown here) in the middle of the domain.

The simulated meridional overturning circulation in the reference climate broadly resembles the observed global overturning (Fig. 2b,e). The circulation in the Atlantic has a clockwise upper cell that represents the AMOC associated with the formation of NADW. Below the idealized AMOC, there is an anti-clockwise lower cell that represents the abyssal overturning circulation, driven by the formation of AABW in the Southern Ocean. In the Pacific, the circulation is overall anti-clockwise although there are two noticeable local streamfunction maxima indicating two different branches of the overturning. The lower maximum represents the Pacific branch of the abyssal overturning circulation, while the upper cell maximum partially balances NADW formation in the Atlantic.

The simulated zonal mean potential density (σ), salinity (S), and potential temperature (θ) distribution are seen to largely reflect the pattern of the circulation (Fig. 2b-g). In the high-latitude Atlantic, we see steep and outcropping isopycnal surfaces indicating the region of NADW formation. The rest of the interior basin on the other hand is well stratified with relatively flat isopycnals. The deep-ocean stratification is primarily set by the relatively fresh but cold AABW underlying the relatively salty but warmer NADW. The Pacific remains well stratified throughout the basin and there is no deep water forming in the high latitudes. The lack of deep water formation in the North Pacific is consistent with present-day conditions, and here follows from more negative

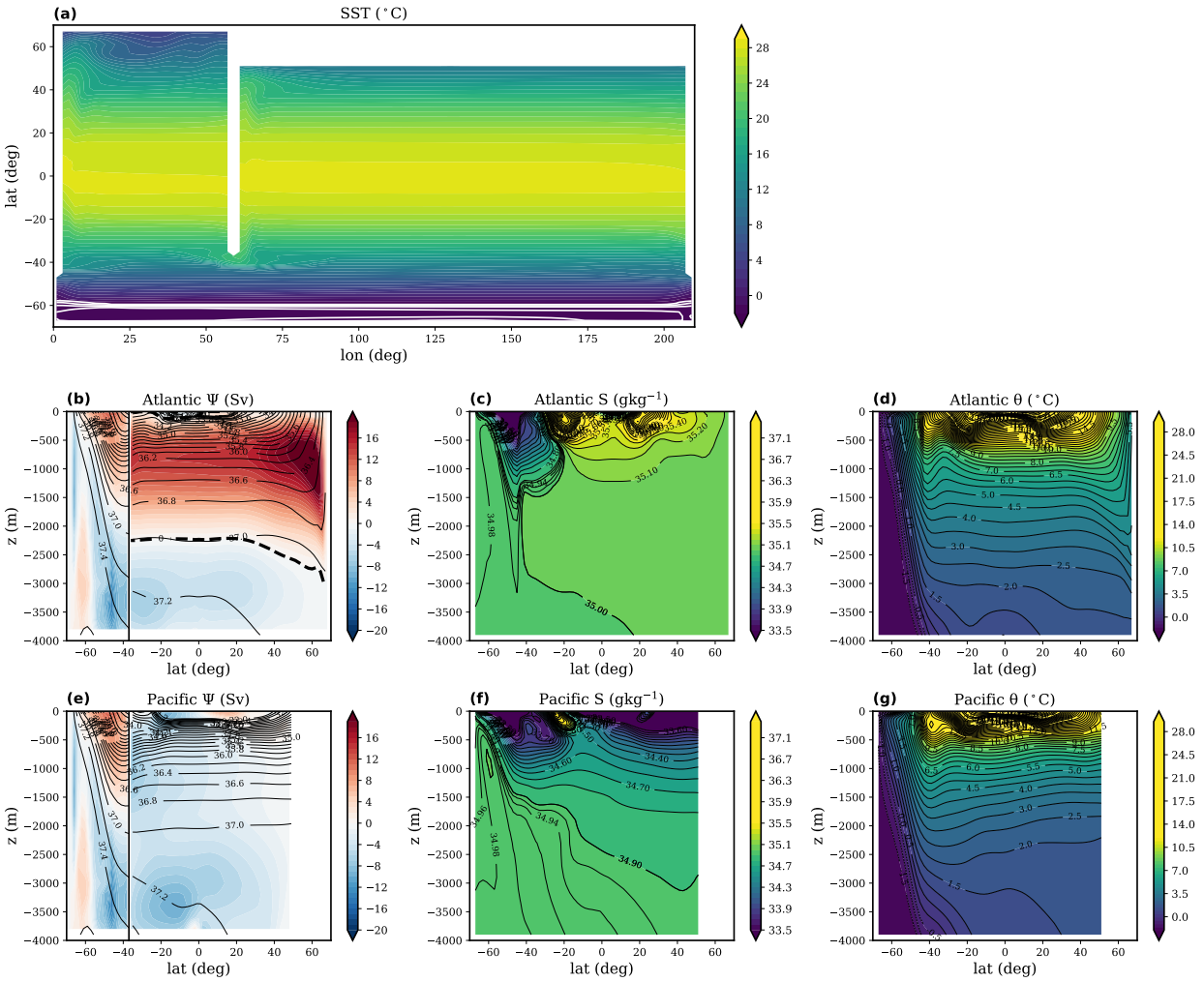

FIG. 2. Reference climate simulated by the idealized ocean-ice climate model. (a) Sea surface temperature (SST; $^{\circ}C$) and sea ice concentration (SIC; white contours with interval of 0.2). (b) Meridional overturning streamfunction, defined as the volume transport by both the resolved flow and parameterized eddies zonally integrated at fixed depth (Ψ; Sv; color shading), and zonally averaged potential density, referenced to 2000dbar (σ; black contours with interval of $0.2 kg m^{-3}$), over the Atlantic basin (north of $36^{\circ}S$) and the Southern Ocean (south of $36^{\circ}S$). (c) Zonally averaged salinity (S; $g kg^{-1}$), and (d) potential temperature (θ; $^{\circ}C$) over the Atlantic basin. Panels (e)-(f) are analog to (b)-(d) but for the Pacific basin. The thick black dashed line in (b) shows the zero contour of the streamfunction, indicating the depth of the AMOC.

$E - P$ in the North Pacific compared to the Atlantic as well as the fact that the Pacific basin does not extend as far north as the Atlantic. Overall, the simulated circulation in the reference climate is

an idealized but reasonable representation of the present-day circulation. In the following we will analyze how it responds to surface warming and cooling.

3. Response to surface temperature changes

To study the circulation response to global surface air temperature change, we conduct a set of simulations where we initialize the model from the last time step of the reference simulation (as shown in Fig. 2) and continue the run with different effective atmospheric temperatures (T_a) adjusted instantaneously at $t = 0$. The T_a profiles differ from the one used for the reference simulation (Fig. 1c) by a uniform temperature offset of $-6°C$, $-4°C$, $-2°C$, $2°C$, $4°C$, and $6°C$, respectively. We focus on the uniform temperature change as it is the simplest starting point, but we have also conducted several simulations with a polar-amplified temperature change which confirm that the results are qualitatively similar and depend mostly on the changes at high latitudes, as previously found in J17 (not shown). An overview of the simulated circulation responses to these abrupt uniform surface temperature changes can be found in Fig. 3, where we plot the time evolution of the meridional overturning streamfunction, Ψ, evaluated at $50°N$ in the North Atlantic.

The response of the circulation is strongly time dependent and varies with the amplitude of surface temperature changes. All simulations show a non-monotonic AMOC response with an initial weakening and shoaling in the warming cases and an initial strengthening and deepening in the cooling cases. In the simulations with relatively small-amplitude surface temperature changes, the circulation eventually equilibrates to a steady state circulation that is similar to the initial state (with changes in the strength and depth of about 1Sv and 50m, respectively). By contrast, in the simulations with relatively large-amplitude surface temperature changes, the AMOC eventually deepens in response to warming, while shoaling in response to cooling. Moreover, oscillations in the strength and the depth of the circulation at the new statistically steady state can be clearly identified in the $6°C$ cooling and warming cases. In the following, we first discuss the transient responses in our simulations to verify that they are consistent with and can be largely explained by the findings in previous studies, in particular, JNM18 and Sun et al. (2020b). We then investigate the mechanisms controlling the diverse responses in the long term, considering first the time-mean and then the oscillations of the circulation.

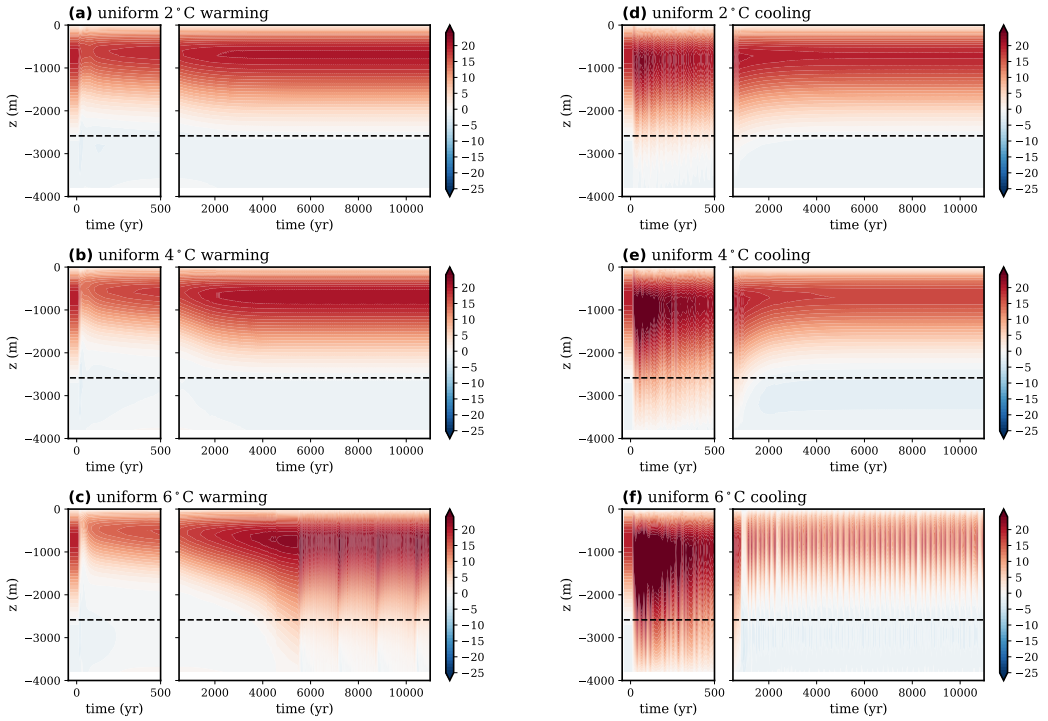

FIG. 3. Hovmoller plots of the Atlantic overturning transport, $\Psi(z)$, at $50°N$ for the simulated responses to different amplitudes of abrupt uniform surface cooling and warming: (a) $2°C$, (b) $4°C$, (c) $6°C$ warming, and (d) $2°C$, (e) $4°C$, (f) $6°C$ cooling. The black dashed line indicates the depth where $\Psi = 0$ at $t = 0$.

a. Transient response of the circulation

The transient response of the Atlantic overturning circulation to the abrupt surface temperature changes shown in Fig. 3 is qualitatively similar to the circulation response in the single-basin simulations reported by JNM18 (c.f. their Fig. 1b). As the surface temperature warms abruptly, the upper cell in the Atlantic basin, i.e., the AMOC, is seen to rapidly become shallower and weaker in the first decades and then recovers slowly on the timescale of centuries (Fig. 3a-c). As the surface temperature cools abruptly, the opposite circulation response is found (Fig. 3d-f). The amplitude of the transient response depends on the amplitude of the surface forcing, with a larger response seen for a larger surface temperature change. For conciseness, we mainly take the uniform $2°C$ warming simulation as the example in the following discussion, since it is likely to be most

relevant for anthropogenic climate change over the 21st century. We then assess the dependence on the forcing amplitude afterwards.

1) Mechanistic interpretation

The transient AMOC response can be related to the adjustment of the deep ocean density distribution, as previously discussed in JNM18 (c.f. their Eq. (1) and Fig. 7). When the surface temperature suddenly changes uniformly across latitudes, the temperatures of the interior ocean initially remain mostly unaffected as they are not exposed to the surface forcing and can only be affected via diffusive heating or changes in the circulation. Only in the high-latitude North Atlantic does deep convection allow the mid-depth temperature to quickly adjust with the surface temperature change. This is illustrated in Fig. 4a-b, which show the evolution of the characteristic temperatures in the high-latitude North Atlantic and the rest of the Atlantic basin, for the uniform $2°C$ warming simulation. The differential warming leads to a positively anomalous (i.e. reduced) north-south temperature contrast in the Atlantic basin (below the depth of the subtropical thermocline) in the first decades and centuries (Fig. 4c), which then translates into a reduced density contrast (Fig. 4d). The reduced meridonal density contrast in turn leads to a reduced meridional overturning, consistent with scaling arguments that assume thermal wind balance together with a relationship between the meridional and zonal buoyancy gradients in the North Atlantic (e.g. JNM18; Gnanadesikan 1999; Nikurashin and Vallis 2012).

Salinity changes can modify the density gradient, but are here found to play a secondary role in the deep ocean density adjustment at the decadal to centennial timescale. To quantify the role of temperature versus salinity changes, we decompose the change in the north-south density contrast into contributions from salinity and temperature (Fig. 4d-f). In the first decades to centuries, the density contrast evolution (Fig. 4d) looks very similar to its temperature-driven part (Fig. 4e), implying a decreased density contrast that drives a weakening of the AMOC. The salt-driven part compensates by causing an increased north-south density contrast at most depths (Fig. 4f), which by itself would be expected to result in a strengthening the AMOC instead. This indicates that the salt-advection feedback is negative in our simulations, arguably consistent with the fact that the net freshwater transport into the Atlantic basin by the Eulerian mean circulation, as defined in Drijfhout et al. (2011), is positive in our reference climate (see e.g. Drijfhout et al. (2011),

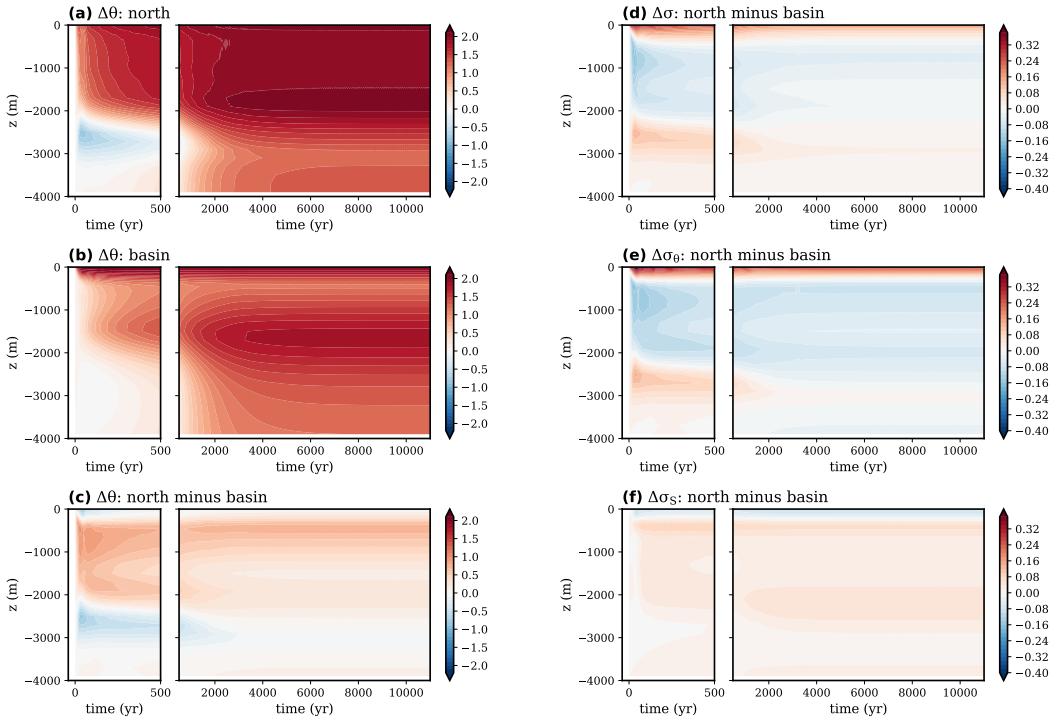

FIG. 4. Hovmoller plot of the temperature and density anomalies, calculated as the difference from the reference climate, which also serves as the initial state, in response to an abrupt uniform $2°C$ surface warming. (a) Temperature anomaly ($\Delta\theta$; $°C$) in the high-latitude North Atlantic (averaged over $60°N$-$68°N$ in the North Atlantic; "north"), (b) in the rest of the Atlantic basin (averaged over $36°S$-$60°N$ in the Atlantic; "basin"), and (c) the north-south contrast ("north" minus "basin"). (d) The anomalous north-south potential density contrast ($\Delta\sigma$; kgm^{-3}), which is further broken down into (e) the contribution from potential temperature change ($\Delta\sigma_\theta$; kgm^{-3}) and (f) the contribution from salinity change ($\Delta\sigma_S$; kgm^{-3}). The potential density anomalies are defined as follows: $\Delta\sigma = \sigma(S_0+\Delta S, \theta_0+\Delta\theta) - \sigma(S_0,\theta_0)$, $\Delta\sigma_S = \sigma(S_0+\Delta S,\theta_0) - \sigma(S_0,\theta_0)$, and $\Delta\sigma_\theta = \sigma(S_0,\theta+\Delta\theta) - \sigma(S_0,\theta_0)$, where the subscript 0 denotes the initial state ($t=0$). The residual, associated with nonlinearities in the equation of state, $\Delta\sigma - \Delta\sigma_S - \Delta\sigma_\theta$, is generally found to be an order of magnitude smaller in all the simulations, so we can assume that $\Delta\sigma \approx \Delta\sigma_S + \Delta\sigma_\theta$.

Liu et al. (2017), but also Mignac et al. (2019)). A positive AMOC freshwater advection into the Atlantic basin is also found in JNM18 and many other comprehensive models, but appears to be at odds with observations (e.g. Drijfhout et al. 2011; Garzoli et al. 2013; Liu et al. 2017).

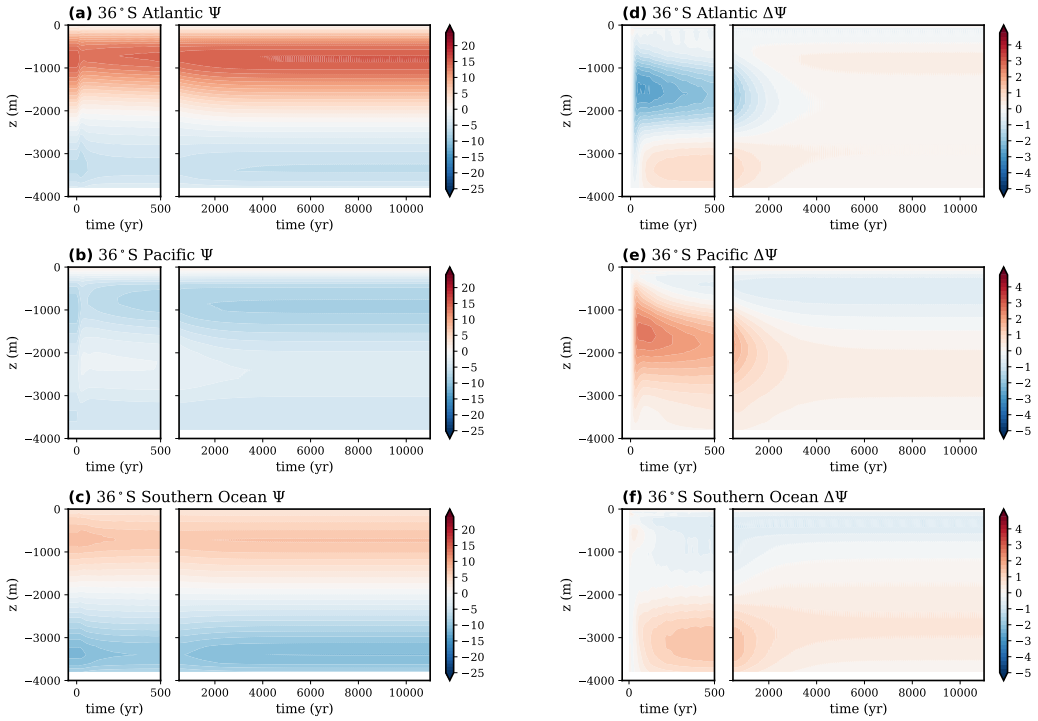

FIG. 5. Hovmoller plot of the overturning transport at $36°S$ in response to an abrupt uniform $2°C$ surface warming: (a) Atlantic, (b) Pacific, (c) Southern Ocean (Atlantic plus Pacific). Panels (d)-(f) are as (a)-(c) but for the respective anomalies relative to the reference climate, which also serves as the initial condition.

2) CONNECTION TO OTHER OCEAN SECTORS

The transient response of the overturning circulation in the Pacific basin and the Southern Ocean in our simulations is qualitatively similar to the circulation response in the two-basin simulations reported by Sun et al. (2020b). To demonstrate the interaction between different parts of the ocean, Fig. 5 shows the time evolution of Ψ evaluated at $36°S$ and integrated over the Atlantic basin, Pacific basin, and the Southern Ocean (equal to the sum of the two basins), respectively.

Consistent with the response in the North Atlantic (Fig. 3a), Ψ evaluated at $36°S$ in the South Atlantic (Fig. 5a) initially weakens and shoals, before recovering on a centennial timescale. However, the AMOC response is weaker in the South Atlantic, implying that part of the AMOC anomaly in the north is balanced by a reduction in existing upwelling over the Atlantic basin.

An initial weakening and shoaling are also seen in the Pacific for the upper anti-clockwise overturning circulation (Fig. 5b). During the first decades after an abrupt surface warming, an anomalous clockwise overturning circulation develops to weaken the existing circulation in the upper Pacific ocean, which largely mirrors and opposes the AMOC change (Fig. 5d-e). The circulation anomaly at the southern end of the Atlantic is thus initially balanced by an anomalous inter-basin exchange, while the net overturning in the Southern Ocean responds more slowly (Fig. 5c,f).

The weaker and slower circulation response in the Southern Ocean relative to the individual basins is consistent with Sun et al. (2020b) and can be understood by considering the strong constraint on the Southern Ocean circulation by its distinct dynamics. Specifically, the circulation in the Southern Ocean, especially for the upper cell, is primarily controlled by the surface winds that are prescribed to be the same in all our simulations. It therefore can only respond to surface warming via changes in the eddy transport, which in turn depends on slower adjustment of the mean isopycnal slopes that are tied to the large-scale stratification in the basins. The inter-basin exchange instead is associated with geostrophic transports driven by the zonal density contrasts along the continental boundary, which can change on the timescales of wave adjustment (Sun et al. 2020b).

Taken together, these results show that the transient responses of the meridional overturning circulation in different parts of the ocean can be largely understood as a direct consequence of the AMOC response to surface forcing. The presence of the inter-basin exchange communicates this signal throughout the global ocean, but does not fundamentally affect the transient response of the AMOC to surface forcing, which can be understood via the North-Atlantic mechanism discussed in the previous subsection.

3) Dependence on the forcing amplitude

The above analysis takes the uniform $2°C$ warming simulation as the example but can also qualitatively explain the other simulations. To more quantitatively compare these simulations, we plot the time evolution of the streamfunction anomalies (relative to $t = 0$), evaluated at the depth of the streamfunction maximum in the control simulation and normalized by the forcing amplitude (with the sign reversed in the cooling cases) in Fig. 6a. We note that the exact values are sensitive to

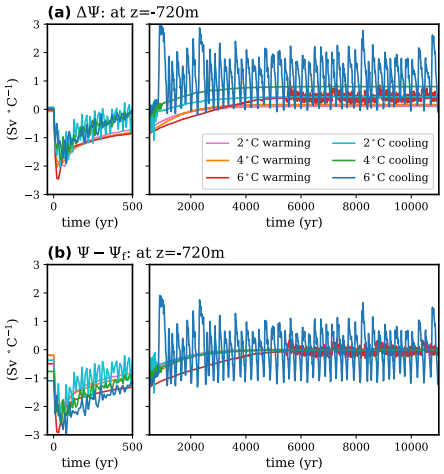

FIG. 6. Time evolution of the streamfunction evaluated at the depth of the streamfunction maximum in the control simulation (z=-720m): (a) the anomaly with respect to $t = 0$, $\Delta\Psi$, (b) the anomaly with respect to the statistically steady state, $\Psi - \Psi_f$, where the subscript f denotes the steady state response defined as the average over the last two thousand years. In all cases the streamfunction anomalies are normalized by the temperature perturbation, and the response for the cooling simulations has a reversed sign.

the depth where the streamfunction is evaluated, with the cooling responses somewhat smaller than the warming responses in the upper ocean and and somewhat larger at greater depth. Nevertheless, to the first order, the streamfunction anomalies scale roughly linearly with the surface temperature perturbation, since the density change in the high-latitude North Atlantic scales approximately linearly with the surface temperature perturbation, as discussed above. In addition, the anomalies in all simulations consistently peak during the first decades, as set by the timescale for the surface temperature perturbations to penetrate through the entire convective column in the North Atlantic high latitudes (JNM18).

The slow, millennial-timescale adjustment of the AMOC following its initial change seems to appear consistently faster in the cooling cases than the warming cases (Fig. 6a), although most of that apparent difference is eliminated if we factor in the differences in their respective new statistically steady states. The approach to the new equilibrium is best examined by considering the anomalies relative to the mean state at the end of the simulation, which is shown in Fig. 6b. In this case the timeseries line up much more closely after 500 years, with the only obvious exception

being the $6°C$ warming case, which takes a significantly longer time to equilibrate. As illustrated by JNM18 and discussed further in the next subsection, the millennial timescale responsible for the long-term change of the AMOC is associated with diffusive adjustment of the abyssal density (c.f. Eq. (4) of JNM18). The estimated timescale from this diffusive scaling argument is about 1200yr for our simulations, which agrees well with the e-folding timescale for the abyssal density adjustment estimated from a fit to the small amplitude simulations (not shown). The adjustment timescale is significantly longer in the $6°C$ warming case, consistent with the expectation that the scaling law of JNM18 breaks down once we move beyond the linear, small amplitude limit. Indeed, a longer timescale is expected with a larger warming as the transient shoaling of the AMOC leads to the isolation of a larger watermass in the abyss, which takes more time to adjust. Consistently, a shorter timescale is found in the $6°C$ cooling case, where the initial deepening of the AMOC allows the watermass in the abyss to adjust faster (JNM18; Stouffer 2004).

b. Long-term response of the time-mean circulation

1) Response to small-amplitude warming and cooling

In the uniform $2°C$ warming simulation, the AMOC eventually recovers and equilibrates at a new steady state that closely resembles the initial conditions (Fig. 3a). A similar result is also found in the case of the uniform $2°C$ cooling simulation, where the circulation at the new steady state remains mostly unchanged from the reference climate (Fig. 3d).

The fact that the simulated circulation barely changes in the steady state responses to small-amplitude uniform surface temperature changes, appears to be inconsistent with the results of J17. Specifically, J17 argued that the AMOC is expected to eventually become shallower in a colder climate as the deep ocean becomes more stratified due to an increase in the salinity of AABW relative to NADW. The latter in turn is an indirect result of enhanced brine rejection from sea ice formation as the surface of the Southern Ocean cools. This salinity effect is also important in our simulations. Yet, we find that the deep ocean temperature changes also play a nonnegligible role in setting the stratification changes and approximately compensates for the salinity effect in our small-amplitude forcing simulations.

To explain the counteracting roles of salinity and temperature in controlling the deep stratification changes, we here use the uniform $2°C$ cooling simulation as the example. As in J17, we focus on

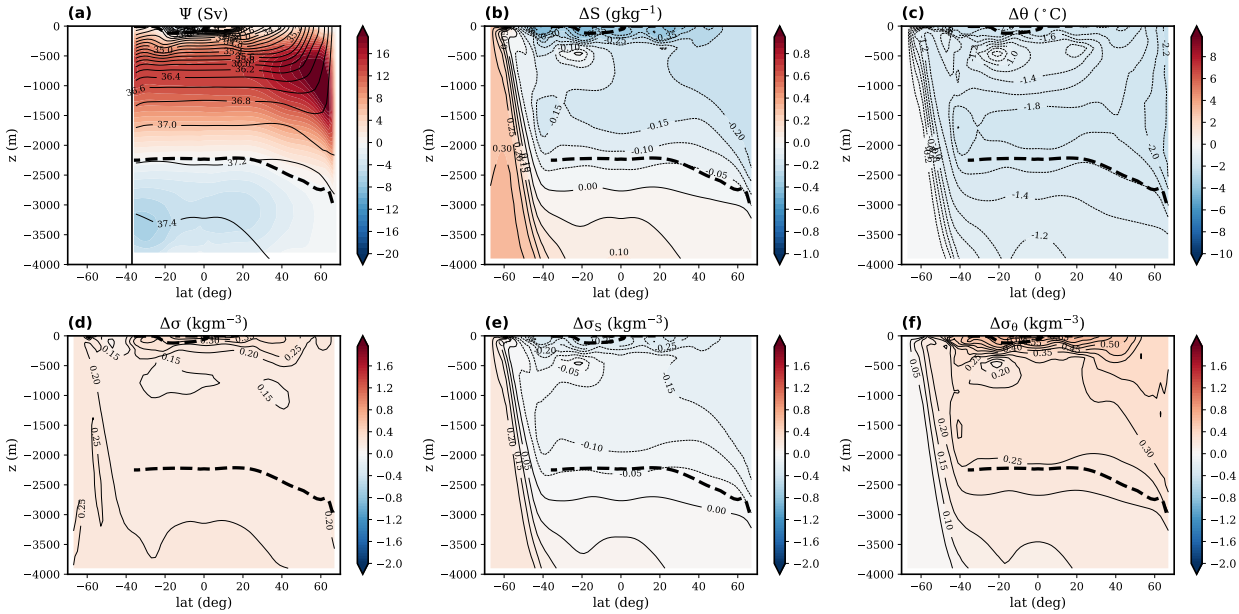

FIG. 7. Time-mean equilibrium results for the Atlantic in the uniform $2°C$ cooling simulation: (a) the overturning transport (Ψ; Sv) and potential density (σ; black contours with interval of $0.2 kgm^{-3}$), (b) the salinity anomaly (ΔS; kgm^{-3}), (c) the potential temperature anomaly ($\Delta\theta$; $°C$), (d) the potential density anomaly ($\Delta\sigma$; kgm^{-3}), (e) the potential density anomaly due to salinity change ($\Delta\sigma_S$; kgm^{-3}), and (f) the potential density anomaly due to potential temperature change ($\Delta\sigma_\theta$; kgm^{-3}). The thick black dashed line indicates the depth of the AMOC in the reference climate, as shown in Fig. 2b.

the steady state response to cooling because of its direct relevance to the Last Glacial Maximum, but we note that similar results (with opposite signs) are found for the small-amplitude warming case. The steady state climate for the uniform $2°C$ cooling simulation is shown in Fig. 7, which confirms that the steady state Atlantic circulation (Fig. 7a) is almost indistinguishable from the reference climate (Fig. 2b) and that this lack of circulation change is associated with a lack of a significant stratification change in the deep Atlantic (Fig. 7d). To illustrate the role of temperature and salinity changes in the stratification change (or lack thereof), we again decompose the change in the density, $\Delta\sigma$, into contributions from salinity, $\Delta\sigma_S$, and contributions from temperature, $\Delta\sigma_\theta$, respectively (as described in Fig. 4).

As shown in Fig. 7e,f, we see that the overall patterns of $\Delta\sigma_S$ and $\Delta\sigma_\theta$ can be characterized by the bulk changes in the two water masses: NADW, which dominates the Atlantic at mid-depth, and AABW, which spans the southern deep corner of the Southern Ocean and the abyssal ocean

in the basin. The spatial distribution of $\Delta\sigma_S$ to a large extent resembles the spatial distribution of ΔS and contributes to an increase in the deep ocean stratification as AABW becomes saltier while the salinity decreases elsewhere due to salt conservation. The spatial distribution of $\Delta\sigma_\theta$, on the other hand, contributes to a decrease of the deep ocean stratification because NADW cools more than AABW in response to a uniform surface cooling. The relatively weak cooling of AABW can be explained by the fact that it is already relatively close to the freezing point in the present-day-like reference climate, such that further cooling merely leads to increased sea ice coverage (c.f. Schmittner et al. 2002; Weber et al. 2007). Adding to the spatial structure of $\Delta\sigma_\theta$ is the temperature dependence of the thermal expansion coefficient. That is, for a given $\Delta\theta$, the climatologically warmer NADW undergoes a larger density change than the climatologically colder AABW (de Boer et al. 2007), although this effect appears to be secondary here.

In summary, the response of the deep stratification and AMOC depth to the surface temperature change is determined by the relative changes in the density of AABW and NADW. Under surface cooling, AABW becomes relatively saltier than NADW, but NADW also becomes relatively colder than AABW, and vice-versa for surface warming. The relative importance of the salinity and temperature effects determines the net response of the deep stratification and hence the change in the AMOC. In our simulations with small-amplitude temperature changes, the temperature effect appears to substantially compensate the salinity effect so that no significant changes are found in the stratification and the circulation.

2) Response to large-amplitude cooling

As the amplitude of the surface cooling is increased, significant changes in the equilibrium circulation are seen in our simulations. As shown in Fig. 3e, the steady state AMOC slightly shoals in the uniform $4°C$ cooling simulation. In the uniform $6°C$ cooling simulation (Fig. 3f), large oscillations of the AMOC are found at the new statistically steady state, which will be addressed in the next section. To get a clearer view of the time-mean response, we plot the circulation and the density structures in the Atlantic averaged over the last two thousand years in Fig. 8. The time-mean depth of the AMOC is seen to become significantly shallower in this coldest climate among our simulations. This shoaling can be explained by an increase in the abyssal stratification, which in turn can be explained by the salinity effect overcoming the temperature effect to set the

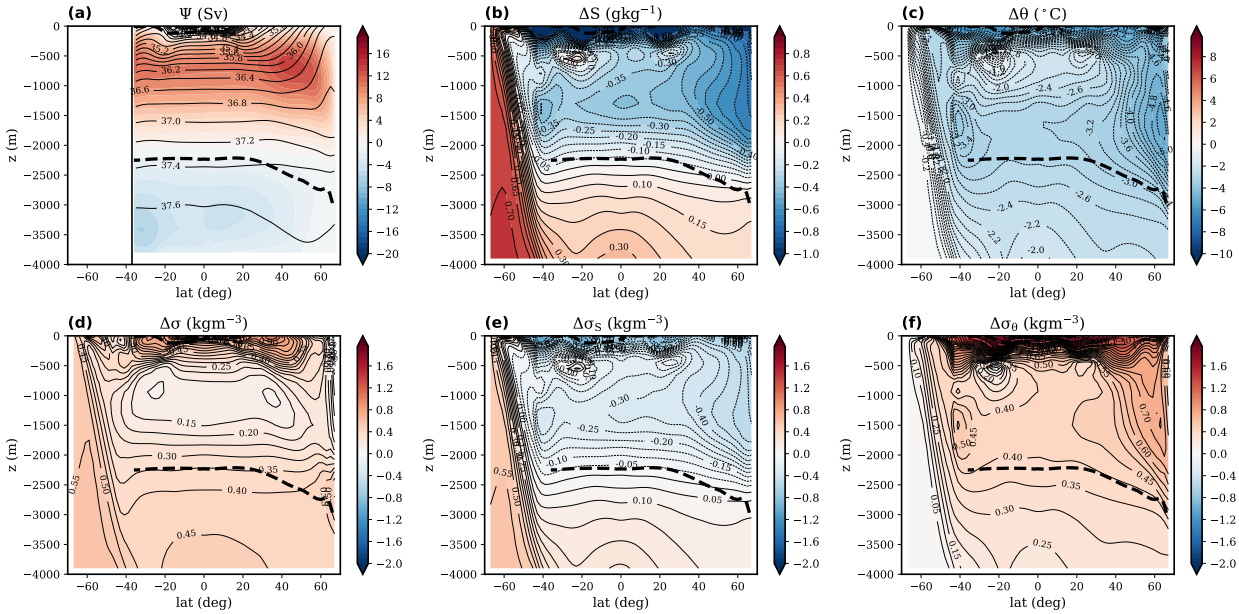

FIG. 8. As in Fig. 7, but for the uniform 6°C cooling simulation.

sign of the time-mean stratification change. Relative to the uniform 2°C cooling (Fig. 7), we see that both the amplitudes of $\Delta\sigma_S$ and $\Delta\sigma_\theta$ increase in response to the uniform 6°C cooling, but the effect of $\Delta\sigma_S$ on the stratification change is stronger. Hence, the deep ocean becomes more stratified and the AMOC shoals, which is qualitatively consistent with the results of J17.

3) RESPONSE TO LARGE-AMPLITUDE WARMING

Although similar mechanisms are at work, the response to large-amplitude warming is not exactly the opposite of the response to large-amplitude cooling. Beginning with the circulation response, we see that the time-mean AMOC averaged over the last two thousand years is deeper when it equilibrates at the new statistically steady state in the uniform 6°C warming simulation (Fig. 8a), and the time-mean deep stratification is reduced (Fig. 9d), which is qualitatively consistent with the opposite changes seen in the uniform 6°C cooling simulation (Fig. 8d). As expected, the salinity changes weaken the deep-ocean stratification due to the reduced sea ice formation in response to surface warming (Fig. 9b,e). The temperature response, on the other hand, is somewhat more complicated (Fig. 9c,f). Rather than working against the change from $\Delta\sigma_S$, $\Delta\sigma_\theta$ contributes to the reduced stratification in the deep ocean because the abyssal ocean warms up more quickly than the upper ocean (Fig. 9c).

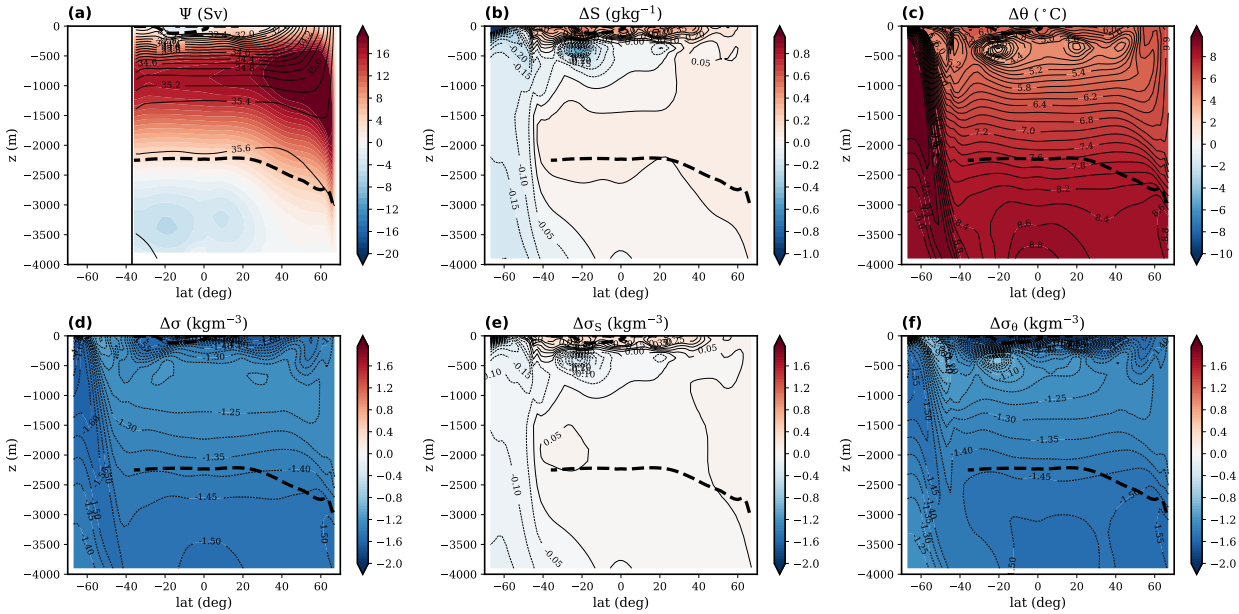

FIG. 9. As in Fig. 7, but for the uniform $6°C$ warming simulation.

To understand the temperature change in the strongest warming case, it is important to note that AABW formation becomes intermittent in this simulation (as will be further described in the next section). When AABW formation is off, NADW mixes with formerly formed AABW to eventually homogenize the temperature and salinity in the deep ocean, as also found in the warming simulation in J17 (c.f. their Fig. S2), where AABW formation is entirely shut off. The abyssal temperature increase in Fig. 8c hence cannot be interpreted as a warming of AABW, but rather represents the intrusion of warmer NADW while AABW formation is off. The temporal variability in the AABW formation and Southern Ocean deep convection is also closely related to the AMOC oscillations observed in this warm climate solution, as will be discussed in the following.

c. Variability of the circulation in the warmest and coldest simulations

After investigating the time-mean responses, we now focus on the AMOC oscillations in the simulations with uniform $6°C$ cooling and $6°C$ warming seen in Fig. 3c,f. The time evolution of the streamfunctions is replotted in Figs. 10a and 11a but for a few cycles near the end of the simulations to better illuminate the nature of the variability.

1) Cold climate variability

We first consider the oscillations in the uniform $6°C$ cooling simulation, where the strength of the AMOC is found to oscillate on a centennial timescale (Fig. 10a). It is seen that, about every two hundred years, the circulation almost disappears for a short time period. Comparison to the timeseries of the convective adjustment index averaged over the northern high latitudes shows that the streamfunction minimum generally appears a few decades after the North Atlantic deep convection is completely off and NADW no longer forms (Fig. 10b). The variability of the AMOC is therefore closely associated with the variability in the convective activity in the North Atlantic.

The North Atlantic convective activity is determined by the interplay of processes controlling the convective instability of the water column in the NADW formation region. Surface cooling via surface heat flux works against the surface warming via poleward heat transport by the circulation to help maintain an unstable temperature stratification in the north. Surface freshening via net precipitation works against surface salinification via advective and convective salt transport to help maintain a stable halocline. In the uniform $6°C$ cooling simulation, the prescribed effective atmospheric temperature (T_a) is lower than the freezing point, leading to the formation of sea ice, which further modulates the heat and salt fluxes, thus enabling the oscillating behavior of convective activity (Fig. 10c-e).

Similar oscillations have been observed in previous modelling studies, with the ocean component ranging from one-dimensional columns (e.g. Singh et al. 2014), two-dimensional (latitude-depth) sections (e.g. De Verdière and Te Raa 2010), to three-dimensional general circulation models configured in either an idealized (e.g. Loving and Vallis 2005) or comprehensive way (e.g. Vettoretti and Peltier 2016). Despite the differences in the models used, these studies have discussed a number of similar mechanisms that appear to be at play also in our simulations. During an oscillation cycle, while convection is on, the deep ocean and with it the region of deep convection cools via surface heat flux until sea ice starts forming (Loving and Vallis 2005; De Verdière and Te Raa 2010; Singh et al. 2014). The sea ice then inhibits heat loss which, together with the positive feedback associated with the formation of a halocline leads to the cessation of convection (De Verdière and Te Raa 2010; Vettoretti and Peltier 2016). While convection is off, the deep ocean warms up, which will eventually destabilize the northern column, at which point convection sets back in (Loving and Vallis 2005; De Verdière and Te Raa 2010; Singh et al. 2014). The convection and associated

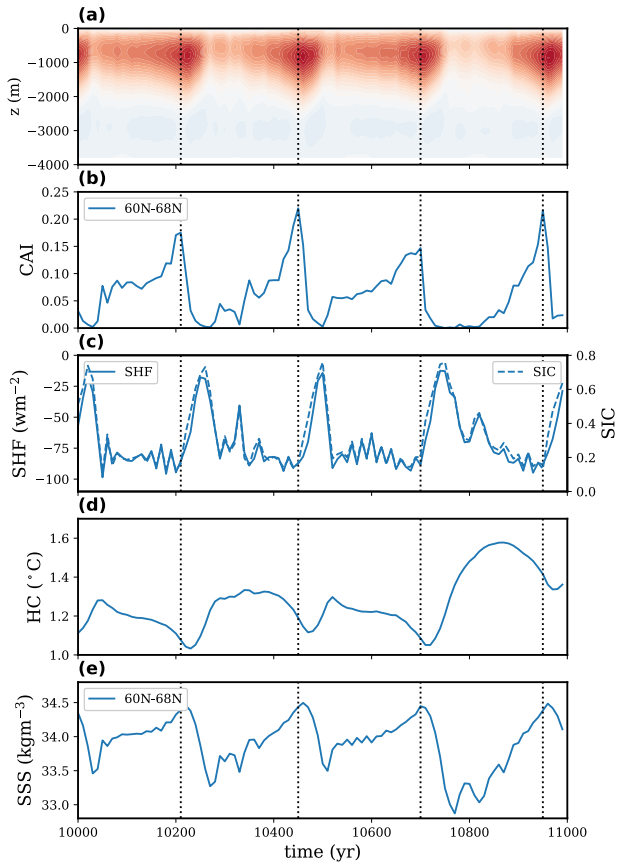

404 FIG. 10. Internal oscillations in the $6°C$ cooling simulation. Variables shown include (a) Atlantic overturning
405 transport (Ψ) at $50°N$ (Sv; using the same colorbar as in Fig. 3), (b) convective adjustment index (CAI), (c)
406 surface heat flux (SHF; Wm^{-2}) and sea ice concentration (SIC), (d) deep ocean heat content (HC; $°C$), and (e) sea
407 surface salinity (SSS; kgm^{-3}). The values for CAI, SHF, SIC, and SSS are obtained by horizontally averaging
408 over $60°N$-$68°N$ in the North Atlantic, while the value for HC is the averaged temperature over the whole Atlantic
409 basin, between $36°S$-$68°N$. The values for CAI and HC are vertical averages taken between $1000m$-$2500m$. The
410 y-axis for the solid lines is on the left, and the y-axis for the dashed lines is on the right. The vertical dotted lines
411 are used to indicate the time of maximum North Atlantic convective activity.

resumption of the AMOC bring in warm, salty water from greater depth and lower latitudes to melt the sea ice and destroy the halocline.

2) Warm climate variability

We now turn to the millennial scale oscillations in the uniform $6°C$ warming simulation (Fig. 11a). About every two thousand years, we see the slow deepening of the AMOC to be abruptly halted by a very short-lived event that is associated with a brief temporary strengthening and a rapid but lasting shoaling. Unlike the oscillations in the cold climate, these warm climate oscillations are associated with variability in AABW formation, as can be seen by looking at the convective adjustment index averaged over the southern polar regions in Fig. 11b. The Southern Ocean remains nonconvective most of the time, but deep convection is intermittently active about every two thousand years. The onset of Southern Ocean deep convection increases the abyssal salinity and leads to the shoaling of the AMOC.

Similar convective variability in the Southern Ocean has also been seen in previous modeling studies, which have suggested a mechanism similar to the one found to be responsible for the variability in the North Atlantic (e.g. Martin et al. 2013; Zhang et al. 2017). As shown in Fig. 11c-e, we see similar variations in the sea ice extent, surface heat loss, deep ocean heat content, and surface salinity in the Southern Ocean polar region as found in the northern hemisphere for the cold climate, although the oscillation is much more regular and the periods during which AABW formation is off are much longer. That is, as sea ice melts and a superpolynya appears in the Southern Ocean, enhanced surface heat loss strengthens the deep convection but also depletes the deep ocean heat content. When the deep ocean becomes cold enough for sea ice to reform, surface heat loss is inhibited and a stable halocline appears, which then inhibits AABW formation, thus leading to a gradual warming of the abyssal ocean, which allows NADW to deepen and fill up the abyss. The warming of the deep Southern Ocean eventually allows convection to resume, repeating the cycle.

A so-far unexplained aspect of this Southern Ocean-originated variability is the sudden strengthening of the AMOC seen shortly after the onset of Southern Ocean deep convection (Fig. 11a), which is also associated with a small but significant enhancement in the convective activity averaged in the northern polar region (Fig. 11b). This sudden enhancement of North Atlantic deep

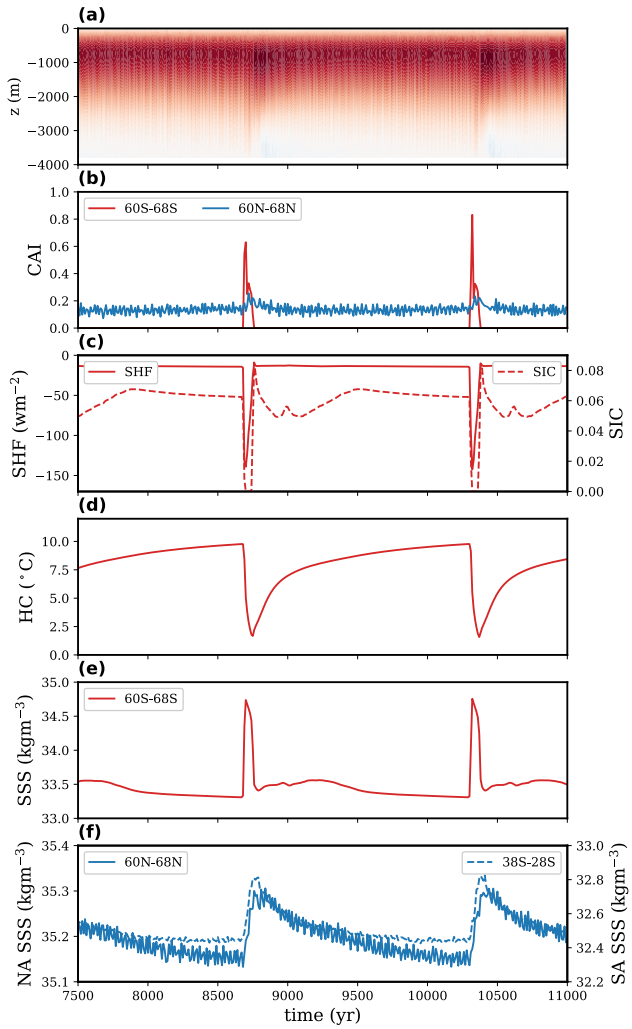

FIG. 11. As in Fig. 10, but for the $6^\circ C$ warming simulation. The values for CAI, SHF, SIC, HC, and SSS, are here obtained by horizontally averaging over $60^\circ S$-$70^\circ S$ in the Southern Ocean to represent the characteristics of Southern Ocean variability and plotted in red. The values for CAI and HC are vertical averages taken between $1000m$-$2500m$. Also shown are in (b) the CAI and in (f) the SSS averaged over $60^\circ N$-$68^\circ N$ in the North Atlantic (NA), and $36^\circ S$-$30^\circ S$ in the South Atlantic (SA).

convection is related to an anomalous increase of the surface salinity in the North Atlantic deep convection region. The positive salt anomaly in turn appears to be advected from the south by

the intermediate water, which becomes saltier during the Southern Ocean convective period (Fig. 11f), likely due to the lack of freshening by sea ice melt (as there is virtually no sea ice in the Southern Ocean during the convective period), and/or the strong mixing with salty deep water that is brought up by the Southern Ocean convection.

It is natural to ask how robust the aforementioned oscillations are across a wider range of climates. To answer this question, we have run some additional simulations, which indicate that although oscillations continue for even warmer and colder climates, their timescales, as well as the relative time spent in the two extreme states, can vary substantially. Perhaps most interesting is that variability originating from the Southern Ocean is still seen in a very warm simulation where the Southern Ocean becomes completely ice free, indicating that sea ice is not necessary, but may be replaced by other positive feedbacks, such as the evolution of a stable halocline driven by surface freshwater forcing when convection is off. Indeed, the salt feedback alone has been found to lead to variability and multiple equilibria when the hemispherical asymmetry of surface freshwater forcing is varied in Wolfe and Cessi (2015). However, we have not seen any indications for multiple equilibria in our simulations with varying surface temperature. Instead, the time mean response seems to be mostly linear with oscillations superimposed in the large amplitude cooling and warming simulations.

4. Discussion

The results presented above show that the transient response in all our simulations and the long term time-mean response in our large-amplitude temperature change simulations are consistent with the mechanisms proposed by JNM18 and J17. However, there remain two main differences between our simulations and the simulations of J17 and JNM18: the time-mean response under small-amplitude temperature changes and the emerging AMOC variability when a new statistically steady climate is achieved in our large-amplitude temperature change simulations. In this section, we discuss how these differences may or may not be linked to the differences in the model setup between J17 and this study, as well as how our idealized model results may shed light on understanding the results of more comprehensive model simulations.

For the long-term time-mean response in our simulations, the change in the AMOC depth depends on the prescribed amplitude of surface temperature change, which modulates the amplitudes of the

partially compensating temperature and salinity changes. By contrast, a more robust relationship between the circulation response and surface forcing is found in J17 and JNM18, where the salt-driven part of the stratification change always dominates the change by the temperature-driven part in equilibrium. A closer look at the simulations in J17 shows that this may be traced back to two different aspects of the model simulations. First, we notice that, for the same amplitude of surface cooling at the high latitudes, the temperature change of NADW is found to be much weaker in the simulations in J17 (c.f. their Fig. 2A-B). This is likely because NADW is already quite cold in the reference climate simulation of J17 (compare their Fig. 2A to our Fig. 2d), and it therefore cannot cool much further before reaching the freezing point. As NADW starts out to be much colder, it also has a smaller thermal expansion coefficient, which further reduces the temperature induced density and stratification change (de Boer et al. 2007).

Second, and perhaps more importantly, we find that the salt-driven stratification increase is much stronger in the simulations of J17 (compare our Fig. 8b to their Fig. 2C-D) because the export and formation of Southern Ocean sea ice are more sensitive to the surface cooling. It remains unclear to us what causes this difference in the sea-ice sensitivity between the two sets of simulations, noting that they share the same sea ice model and similar model configurations, except for the basin geometry, small differences in the boundary conditions, and coarser resolution (section 2). We have conducted additional simulations to better understand the effect of the various differences in the model setup. While we found resolution to have a negligible effect, changing the model geometry or boundary conditions in isolation affects not only the sensitivity of the sea ice export to surface temperature changes, but also strongly alters the mean climate state (cf. Nadeau and Jansen 2020). As a result, we found it impossible to infer in how far the change in the sea ice sensitivity is attributable to the model configuration itself or differences in the reference climate. While we were unable to pinpoint how exactly various modelling choices affect the sensitivity of Southern Ocean sea ice export, we note that variations in the Southern Ocean sea ice response to surface cooling have also been identified as a key factor to explain variations in the change of AMOC depth across PMIP simulations with Last Glacial Maximum boundary conditions (Marzocchi and Jansen 2017), highlighting the Antarctic sea ice response as a key uncertainty governing the AMOC response during past and future climate changes.

Although not a focus of that study, AMOC variability is also observed in the cold climate simulation of J17, yet with a smaller variance and shorter time-scale. As discussed earlier, we have conducted additional simulations that show that the characteristics of the cold climate variability are sensitive to the imposed temperature perturbations and other aspects of the model configuration that control the mean climate, again making it difficult to attribute differences in the oscillations to specific aspects of the model setup and/or associated reference climates. However, in all simulations, this variability appears only when the North Atlantic is cold enough for sea ice to form, confirming that North Atlantic sea ice plays an important role in the variability. Previous modeling studies have argued that similar oscillations may explain Dansgaard-Oeschger events during the glacial climate (e.g. Loving and Vallis 2005; De Verdière and Te Raa 2010; Singh et al. 2014; Vettoretti and Peltier 2016). The sensitivity of the oscillation to North Atlantic sea ice cover is broadly consistent with the fact that Dansgaard-Oeschger oscillations are seen in the glacial climate but disappear when entering the warmer Holocene.

The variability in our warmest simulation does not appear in J17's warm climate simulation, where Southern Ocean convection is permanently off and the Southern Ocean surface temperatures stay permanently above the freezing point. Variability associated with fluctuations in the Southern Ocean convection and polynya formation has instead been seen in pre-industrial simulations in some state-of-the-art CMIP models (e.g. Held et al. 2019; Sellar et al. 2020). To our knowledge, most models exhibiting similar variability are coupled ice-ocean-atmosphere models involving, for instance, changes in atmospheric winds. Our ice-ocean-only simulations suggest that atmospheric feedbacks are, however, not necessary to obtain similar oscillations, and allow for a cleaner isolation of the mechanisms. It is worth noting, however, that the Southern Ocean convection in our simulations occurs over the open ocean rather than along a continental shelf. This unrealistic aspect of our model is also shared by most other models, and it is likely that the simulated variability is sensitive to this shortcoming (e.g. Heuzé et al. 2013; Reintges et al. 2017). Therefore, it remains debated whether this variability has a real-world analog or is a spurious model phenomenon. Yet, some have argued for its potential importance in explaining the present-day and future changes of Southern Ocean climate, calling for more efforts to better understand this phenomenon (e.g. De Lavergne et al. 2014; Campbell et al. 2019; Zhang et al. 2019, 2021). Our results, indicating that

variability in AABW formation may be particularly likely in a warmer climate, provide additional motivation for future work on this topic.

To summarize, while our results are based on an idealized model and the specifics of the long-term response and oscillations are likely to be model and mean-state dependent, we believe that the identified mechanisms can help draw general inferences about comprehensive models and the real world where similar climate features have been identified. That being said, we note that there remain many differences between our simulations and the real world that need to be considered. One obvious example is the potential effect of open-ocean convection versus deep water formation on the Antarctic shelves, discussed above. Another example is the role of diapycnal mixing, whose strength can quantitatively affect the sensitivity of the AMOC to surface buoyancy forcing (cf. Eq. (10) of Jansen and Nadeau (2016) and see also Sun et al. (2020a) and Baker et al. (2021)). Diapycnal mixing is prescribed in our model simply as a function of depth, but in the real world should be enhanced near topographic features, which may be important for setting the abyssal stratification and circulation (e.g. Ferrari et al. 2016; Drake et al. 2020). Moreover, diapycnal mixing may itself decrease with increasing abyssal stratification due to higher energy dissipation required to mix a more strongly stratified water column. This feedback may further amplify the sensitivity of AMOC depth and strength to abyssal stratification (e.g. Nadeau and Jansen 2020).

5. Conclusions

This work examines a set of coupled ice-ocean model simulations with an idealized two-basin geometry to study the mechanisms governing the response of the Atlantic Meridional Overturning Circulation (AMOC) to surface temperature changes, while keeping other forcings fixed. We impose an instantaneous, uniform temperature change ranging from $-6°C$ to $6°C$ on the model's effective atmospheric temperature to obtain a series of sensitivity runs. Using these simulations, we investigate the responses of the circulation and discuss in which aspects they agree or disagree with the mechanisms proposed by previous studies. Our key findings are summarized in the following:

- As previously found in JNM18, the transient response to surface warming involves a weakening of the AMOC, driven by rapid warming in the northern convective regions that leads interior warming at low latitudes (and vice versa for cooling). An anomalous overturning circulation, which largely compensates for the change in the AMOC, also emerges in the Pacific basin,

as previously discussed by Sun et al. (2020b). The adjustment timescale for the AMOC to equilibrate generally follows the diffusive scaling proposed in JNM18 for relatively small perturbations.

- As previously found in J17, the time mean AMOC eventually shoals under large-amplitude surface cooling as the salinification of AABW due to sea ice formation increases the deep ocean stratification, and vice versa for large-amplitude warming. However, a similar result is not seen when the change in surface temperature is small, since the salt-driven stratification change is largely compensated by an opposing change in the thermal stratification, as the NADW temperature responds more strongly to the surface temperature change than the AABW temperature, which always stays around the freezing point. Since NADW temperature and the sensitivity of sea ice export to climatic changes are likely to differ across models, this indicates that the sensitivity of the AMOC is also likely to be model dependent.

- Significant internal variability of the AMOC is seen in our coldest and warmest simulations. The cold climate variability is directly related to variability in the North Atlantic deep convection and may resemble Dansgaard-Oeschger Oscillations observed during the glacial climate, while the warm climate variability is related to convective activity in the Southern Ocean. Both involve variations in sea ice extent, surface heat loss, deep ocean heat content, and surface salinity in the convective regions, sharing many similarities with variability that has previously been identified in more comprehensive models. This indicates that idealized ocean-ice models have the basic ingredients for this low frequency variability, although the specific climate regime where the variability emerges as well as the specific frequency of the oscillation are likely to be model dependent.

The mechanisms discussed in this study focus only on the circulation response to changes in global surface temperature and associated sea ice changes. As the atmosphere warms or cools, we also expect changes in evaporation and precipitation via changes in the global hydrological cycle (e.g. Manabe and Stouffer 1994; Cael and Jansen 2020) as well as potential changes in run-off from ice-sheets (e.g. Stouffer et al. 2006; Bakker et al. 2016; Sadai et al. 2020). How these changes in freshwater forcing further modify the physical picture discussed here remains an important research question for future work.

Acknowledgments. Computational resources for this project were generously provided by the University of Chicago Research Computing Center. C.Y.C. and M.F.J. acknowledge support from NSF Award OCE-1846821.

Data availability statement. The MITgcm is publicly available on GitHub at `https://github.com/MITgcm`, and the configuration files used for this study are available at `https://doi.org/10.5281/zenodo.6056143`.

References

Baker, J. A., A. J. Watson, and G. K. Vallis, 2020: Meridional Overturning Circulation in a Multi-basin Model. Part I: Dependence on Southern Ocean Buoyancy Forcing. *Journal of Physical Oceanography*, **50 (5)**, 1159–1178.

Baker, J. A., A. J. Watson, and G. K. Vallis, 2021: Meridional overturning circulation in a multibasin model. part ii: Sensitivity to diffusivity and wind in warm and cool climates. *Journal of Physical Oceanography*, **51 (6)**, 1813–1828.

Bakker, P., and Coauthors, 2016: Fate of the atlantic meridional overturning circulation: Strong decline under continued warming and greenland melting. *Geophysical Research Letters*, **43 (23)**, 12,252–12,260.

Bryan, K., 1984: Accelerating the convergence to equilibrium of ocean-climate models. *Journal of Physical Oceanography*, **14 (4)**, 666 – 673.

Burke, A., A. L. Stewart, J. F. Adkins, R. Ferrari, M. F. Jansen, and A. F. Thompson, 2015: The glacial mid-depth radiocarbon bulge and its implications for the overturning circulation. *Paleoceanography*, **30 (7)**, 1021–1039.

Cael, B. B., and M. F. Jansen, 2020: On freshwater fluxes and the atlantic meridional overturning circulation. *Limnology and Oceanography Letters*, **5 (2)**, 185–192.

Campbell, E. C., E. A. Wilson, G. K. Moore, S. C. Riser, C. E. Brayton, M. R. Mazloff, and L. D. Talley, 2019: Antarctic offshore polynyas linked to southern hemisphere climate anomalies. *Nature*, **570 (7761)**, 319–325.

Cessi, P., 2019: The Global Overturning Circulation. *Annual Review of Marine Science*, **11 (1)**, 249–270.

Cheng, W., J. C. H. Chiang, and D. Zhang, 2013: Atlantic Meridional Overturning Circulation (AMOC) in CMIP5 Models: RCP and Historical Simulations. *Journal of Climate*, **26 (18)**, 7187 – 7197.

Curry, W. B., and D. W. Oppo, 2005: Glacial water mass geometry and the distribution of ÎŽ13c of Î£co2 in the western atlantic ocean. *Paleoceanography*, **20 (1)**, PA1017.

de Boer, A. M., D. M. Sigman, J. R. Toggweiler, and J. L. Russell, 2007: Effect of global ocean temperature change on deep ocean ventilation. *Paleoceanography*, **22 (2)**, PA2210.

De Lavergne, C., J. B. Palter, E. D. Galbraith, R. Bernardello, and I. Marinov, 2014: Cessation of deep convection in the open southern ocean under anthropogenic climate change. *Nature Climate Change*, **4 (4)**, 278–282.

De Verdière, A. C., and L. Te Raa, 2010: Weak oceanic heat transport as a cause of the instability of glacial climates. *Climate dynamics*, **35 (7-8)**, 1237–1256.

Drake, H. F., R. Ferrari, and J. Callies, 2020: Abyssal circulation driven by near-boundary mixing: Water mass transformations and interior stratification. *Journal of Physical Oceanography*, **50 (8)**, 2203 – 2226.

Drijfhout, S. S., S. L. Weber, and E. van der Swaluw, 2011: The stability of the moc as diagnosed from model projections for pre-industrial, present and future climates. *Climate Dynamics*, **37 (7-8)**, 1575–1586.

Ferrari, R., A. Mashayek, T. J. McDougall, M. Nikurashin, and J.-M. Campin, 2016: Turning ocean mixing upside down. *Journal of Physical Oceanography*, **46 (7)**, 2239 – 2261.

Ferrari, R., L.-P. Nadeau, D. P. Marshall, L. C. Allison, and H. L. Johnson, 2017: A model of the ocean overturning circulation with two closed basins and a reentrant channel. *Journal of Physical Oceanography*, **47 (12)**, 2887 – 2906.

Garzoli, S. L., M. O. Baringer, S. Dong, R. C. Perez, and Q. Yao, 2013: South atlantic meridional fluxes. *Deep Sea Research Part I: Oceanographic Research Papers*, **71**, 21–32.

Gent, P. R., and J. C. McWilliams, 1990: Isopycnal Mixing in Ocean Circulation Models. *Journal of Physical Oceanography*, **20 (1)**, 150–155.

Gnanadesikan, A., 1999: A Simple Predictive Model for the Structure of the Oceanic Pycnocline. *Science*, **283 (5410)**, 2077–2079.

Held, I. M., and Coauthors, 2019: Structure and performance of gfdl's cm4.0 climate model. *Journal of Advances in Modeling Earth Systems*, **11 (11)**, 3691–3727.

Heuzé, C., K. J. Heywood, D. P. Stevens, and J. K. Ridley, 2013: Southern ocean bottom water characteristics in cmip5 models. *Geophysical Research Letters*, **40 (7)**, 1409–1414.

Jansen, M. F., 2017: Glacial ocean circulation and stratification explained by reduced atmospheric temperature. *Proceedings of the National Academy of Sciences*, **114 (1)**, 45–50.

Jansen, M. F., and L.-P. Nadeau, 2016: The Effect of Southern Ocean Surface Buoyancy Loss on the Deep-Ocean Circulation and Stratification. *Journal of Physical Oceanography*, **46 (11)**, 3455–3470.

Jansen, M. F., L.-P. Nadeau, and T. M. Merlis, 2018: Transient versus equilibrium response of the ocean's overturning circulation to warming. *Journal of Climate*, **31 (13)**, 5147 – 5163.

Jones, C. S., and P. Cessi, 2016: Interbasin transport of the meridional overturning circulation. *Journal of Physical Oceanography*, **46 (4)**, 1157 – 1169.

Liu, W., S.-P. Xie, Z. Liu, and J. Zhu, 2017: Overlooked possibility of a collapsed atlantic meridional overturning circulation in warming climate. *Science Advances*, **3 (1)**, e1601 666.

Liu, Z., 2006: Glacial thermohaline circulation and climate: Forcing from the north or south? *Advances in Atmospheric Sciences*, **23 (2)**, 199–206.

Loving, J. L., and G. K. Vallis, 2005: Mechanisms for climate variability during glacial and interglacial periods. *Paleoceanography*, **20 (4)**, PA4024.

Lynch-Stieglitz, J., and Coauthors, 2007: Atlantic meridional overturning circulation during the last glacial maximum. *Science*, **316 (5821)**, 66–69.

Manabe, S., and R. J. Stouffer, 1994: Multiple-century response of a coupled ocean-atmosphere model to an increase of atmospheric carbon dioxide. *Journal of Climate*, **7 (1)**, 5–23.

Marshall, J., A. Adcroft, C. Hill, L. Perelman, and C. Heisey, 1997: A finite-volume, incompressible Navier Stokes model for studies of the ocean on parallel computers. *Journal of Geophysical Research: Oceans*, **102 (C3)**, 5753–5766.

Martin, T., W. Park, and L. M., 2013: Multi-centennial variability controlled by Southern Ocean convection in the Kiel Climate Model. *Climate dynamics*, **40 (7)**, 2005–2022.

Marzocchi, A., and M. F. Jansen, 2017: Connecting antarctic sea ice to deep-ocean circulation in modern and glacial climate simulations. *Geophysical Research Letters*, **44 (12)**, 6286–6295.

Mignac, D., D. Ferreira, and K. Haines, 2019: Decoupled freshwater transport and meridional overturning in the south atlantic. *Geophysical Research Letters*, **46 (4)**, 2178–2186.

Nadeau, L.-P., R. Ferrari, and M. F. Jansen, 2019: Antarctic sea ice control on the depth of north atlantic deep water. *Journal of Climate*, **32 (9)**, 2537 – 2551.

Nadeau, L.-P., and M. F. Jansen, 2020: Overturning circulation pathways in a two-basin ocean model. *Journal of Physical Oceanography*, **50 (8)**, 2105 – 2122.

Nikurashin, M., and R. Ferrari, 2013: Overturning circulation driven by breaking internal waves in the deep ocean. *Geophysical Research Letters*, **40 (12)**, 3133–3137.

Nikurashin, M., and G. Vallis, 2012: A Theory of the Interhemispheric Meridional Overturning Circulation and Associated Stratification. *Journal of Physical Oceanography*, **42 (10)**, 1652–1667.

Reintges, A., T. Martin, M. Latif, and W. Park, 2017: Physical controls of southern ocean deep-convection variability in cmip5 models and the kiel climate model. *Geophysical Research Letters*, **44 (13)**, 6951–6958.

Sadai, S., A. Condron, R. DeConto, and D. Pollard, 2020: Future climate response to antarctic ice sheet melt caused by anthropogenic warming. *Science advances*, **6 (39)**, eaaz1169.

Schmittner, A., K. J. Meissner, M. Eby, and A. J. Weaver, 2002: Forcing of the deep ocean circulation in simulations of the last glacial maximum. *Paleoceanography*, **17 (2)**, 5–1–5–15.

Sellar, A. A., and Coauthors, 2020: Implementation of u.k. earth system models for cmip6. *Journal of Advances in Modeling Earth Systems*, **12 (4)**, e2019MS001 946.

Singh, H. A., D. S. Battisti, and C. M. Bitz, 2014: A heuristic model of dansgaard–oeschger cycles. part i: Description, results, and sensitivity studies. *Journal of climate*, **27 (12)**, 4337–4358.

Stouffer, R. J., 2004: Time scales of climate response. *Journal of Climate*, **17 (1)**, 209 – 217, https://doi.org/10.1175/1520-0442(2004)017<0209:TSOCR>2.0.CO;2, URL https://journals.ametsoc.org/view/journals/clim/17/1/1520-0442_2004_017_0209_tsocr_2.0.co_2.xml.

Stouffer, R. J., and Coauthors, 2006: Investigating the causes of the response of the thermohaline circulation to past and future climate changes. *Journal of Climate*, **19 (8)**, 1365 – 1387.

Sun, S., I. Eisenman, L. Zanna, and A. L. Stewart, 2020a: Surface constraints on the depth of the atlantic meridional overturning circulation: Southern ocean versus north atlantic. *Journal of Climate*, **33 (8)**, 3125 – 3149.

Sun, S., A. F. Thompson, and I. Eisenman, 2020b: Transient overturning compensation between atlantic and indo-pacific basins. *Journal of Physical Oceanography*, **50 (8)**, 2151 – 2172.

Thompson, A. F., A. L. Stewart, and T. Bischoff, 2016: A multibasin residual-mean model for the global overturning circulation. *Journal of Physical Oceanography*, **46 (9)**, 2583 – 2604.

Vettoretti, G., and W. R. Peltier, 2016: Thermohaline instability and the formation of glacial north atlantic super polynyas at the onset of dansgaard-oeschger warming events. *Geophysical Research Letters*, **43 (10)**, 5336–5344.

Weber, S. L., and Coauthors, 2007: The modern and glacial overturning circulation in the Atlantic ocean in PMIP coupled model simulations. *Climate of the Past*, **3 (1)**, 51–64.

Wolfe, C. L., and P. Cessi, 2015: Multiple regimes and low-frequency variability in the quasi-adiabatic overturning circulation. *Journal of Physical Oceanography*, **45 (6)**, 1690 – 1708.

Zhang, L., T. L. Delworth, W. Cooke, H. Goosse, M. Bushuk, Y. Morioka, and X. Yang, 2021: The dependence of internal multidecadal variability in the southern ocean on the ocean background mean state. *Journal of Climate*, **34 (3)**, 1061 – 1080.

Zhang, L., T. L. Delworth, W. Cooke, and X. Yang, 2019: Natural variability of southern ocean convection as a driver of observed climate trends. *Nature Climate Change*, **9 (1)**, 59–65.

748 Zhang, L., T. L. Delworth, and L. Jia, 2017: Diagnosis of Decadal Predictability of Southern
749 Ocean Sea Surface Temperature in the GFDL CM2.1 Model. *Journal of Climate*, **30 (16)**, 6309
750 – 6328.